Article

Not peer-reviewed version

Biomineralization Process in Three-Dimensional Scaffolds Based on Bacterial Nanocellulose for Bone Tissue Engineering: Chemi-Cal and Morphological Features, and Stem Cell Differentiation

Ana Cañas-Gutiérrez *, Lenka Toro, Cristina Fornaguera, Salvador Borrós, Marlon Osorio, Cristina Castro-Herazo, David Arboleda-Toro

Posted Date: 27 February 2023

doi: 10.20944/preprints202302.0431.v1

Keywords: nanocomposites; bacterial nanocellulose; microporosity; biomineralization process and bone regeneration

Article

Biomineralization Process in Three-Dimensional Scaffolds Based on Bacterial Nanocellulose for Bone Tissue Engineering: Chemical and Morphological Features, and Stem Cell Differentiation

Ana Cañas-Gutiérrez [1,*], Lenka Toro [2,3], Cristina-Fornaguera [4], Salvador-Borrós [4], Marlon Osorio [1], Cristina Castro-Herazo [1] and David Arboleda-Toro [5]

[1] Research Group on New Materials (GINUMA), Faculty of Engineering, Universidad Pontificia Bolivariana, Circular 1 No. 70-01, Medellín, Colombia
[2] Biomedical Engineering Research Group (GIBEC), EIA University, Km 2 + 200 on the way to the José María Córdova airport, Alto de Las Palmas, Envigado, Colombia
[3] Cancer Research Institute, Biomedical Research Center, University Science Park for Biomedicine, Slovak Academy of Sciences, 84505 Bratislava, Slovakia.
[4] Grup d'Enginyeria de Materials (Gemat), Institut Químic de Sarrià (IQS), Universitat. Ramon Llull (URL), Via Augusta 390, 08017 Barcelona, Spain
[5] Group of Biosocial Studies of the Body-EBSC-, Faculty of Dentistry, Universidad de Antioquia Calle 64 No. 52-59, Medellín, Colombia
* Correspondence: ana.canas@upb.edu.co

Abstract: Bacterial nanocellulose (BNC) surface has a negative charge that allows the adsorption of calcium ions to initiate the nucleation of different calcium phosphate phases. The aim of this study was to investigate different methods of mineralization on three-dimensional microporous bacterial nanocellulose, to mimetize the composition, structure, and biomechanical properties of natural bone. To generate 3D microporous biomaterial, the porogen particles were incorporated during the BNC fermentation with the strain *Komagataeibacter medellinensis.* Calcium phosphates (CPs) were deposited on BNC scaffolds by five alternating immersing cycles with calcium and phosphate solutions. Scanning electron microscopy micrograph showed that the scaffolds have different pore sizes, between 70 and 350 μm, but the porous interconnectivity was affected by the biomineralization method and time. The crystals on the BNC surface are shown to be rod-shaped with a calcium phosphate ratio similar to that of immature bone, increasing from 1.13 to 1.6 with cycle numbers. The main mineral phases obtained by X-ray diffraction were Octacalcium Dihydrogen Hexakis (phosphate (V)) Pentahydrate (OCP). In vitro cell studies showed good cellular adhesion and higher cell viability to 95% in all the scaffolds. Osteogenic differentiation of human bone marrow mesenchymal stem cells on the scaffolds was evaluated by bone expression markers like alkaline phosphatase, osteocalcin, and osteopontin. In conclusion, it is possible to prepare 3D BNC scaffolds with controlled microporosity, which could allow osteoblast adhesion, proliferation, and differentiation.

Keywords: nanocomposites; bacterial nanocellulose; microporosity; biomineralization process and bone regeneration

1. Introduction

Tissue engineering seeks, through the development of new biomaterials, to create a microenvironment that activates the self-cells of the patient to promote their regeneration. This field uses biomimetics as one of its strategies to develop scaffolds that mimic the extracellular matrix (ECM) of native tissues, and thus, improve the biological affinity between cells and the materials that

serve as substrates [1,2]. Regarding to mimic ECM of bone tissue, it is important to emphasize that bone is composed of two phases: an organic and an inorganic phase, both fulfilling a specific function in tissue homeostasis. For instance, the mechanical performance of the organic phase composed of type I collagen and other proteins impart flexibility to the tissue, while the inorganic phase composed of calcium phosphates provides rigidity [3], and the compositional and biological characteristics of bone, it is important to emphasize that this is a highly dynamic tissue, which varies considerably during the bone maturation process and constantly during the bone remodeling process [4–6].

Therefore, when designing a bone graft, it must be considered that the biomaterial to be used must activate the mechanisms that involve the bone repair and regeneration process, which are: osteoinduction, osteoconduction and osteogenesis [7,8]. From this, the new graft must stimulate the osteoinduction process through the differentiation of mesenchymal stem cells (MSCs) into osteoblasts, which are mature bone-forming cells. Additionally, the material should promote osteogenesis through the formation of new bone at the injury site [9,10]. Finally, the bone graft must have a microporous three-dimensional structure, which scaffolds the function of osteoconductivity by guiding bone growth, allowing vascular invasion and cellular infiltration within the interconnected pores [11].

Currently, autologous bone grafts are the most used for the regeneration of bone structures. These consist of material extracted from another site of the same patient such as the bone of the pelvic region, tibia, skull, rib, and jaw [12,13]. This procedure is highly invasive and due to its high morbidity to the intervened tissues, it carries a potential risk of complications that include pain, bleeding, infection, fracture, scars, chronic pain, or paresthesia. Allografts and xenografts have also been used for hard tissue treatments, but these materials have shown immune rejection responses and are related to undesired infections, so specialists avoid using them [10,14].

Due to the disadvantages of currently available bone grafts, the search for new alternatives in terms of designing biomaterials that can be used as grafts or bone substitutes is still ongoing. Currently, biodegradable natural polymers are very popular in bone tissue engineering [1], and although these allow cell proliferation, they have rapid reabsorption rates, preventing cells from forming new tissue properly [15]. This is a current medical need that bacterial nanocellulose (BNC) can address, as it is a natural polymer that is not biodegradable in vivo [16,17], and which can be used as a replacement of the matrix (scaffold) with very good physical, chemical and biocompatibility properties required to restore normal tissue function [18].

One of the most attractive features of BNC is its unique nanofibrillary structure that mimics the structure of the native extracellular matrix, allowing rapid tissue healing and regeneration [19]. In addition, BNC has high reproducibility and does not contain any components of animal origin that can cause allergic or immunogenic reactions [20]. Therefore, it has been studied for various applications such as dressings for skin burns [21], 3D prototypes in various forms such as the external ear [22], and menisci of knees [23], and tubes with different diameters, lengths, and wall thickness, for use as artificial blood vessels for microsurgery [24].

Specifically, in bone tissue engineering, BNC has been used in dental and oral applications, primarily as a barrier material in guided tissue regeneration (GTR). The function of the cellulose membrane in this application is to guide the regeneration of the alveolar bone in periodontal diseases, allowing the bone cells to grow and form a functional tissue [25,26]. On the other hand, unmodified BNC has also been evaluated as a porous three-dimensional scaffold in bone regeneration [27] and as a scaffold to induce the differentiation of bone marrow mesenchymal stem cells (EqMSC) into osteoblasts [28].

Bacterial nanocellulose by itself has a low ability to bind directly to bone, but its versatility allows it to be modified with other materials such as hydroxyapatite (HA), calcium phosphate (CaP) variants or bioactive glasses, to increase its bioactivity and improve the process of bone regeneration [29]. Some scientific reports on two-dimensional, non-porous composites based on BNC/HA and BNC/CaP, have shown that these composites have excellent moldability and biocompatibility properties for bone tissue regeneration applications [30,31]. *In vitro*, BNC has been shown to stimulate bone cell adhesion, migration, proliferation, and differentiation [32–35], and in vivo BNC has shown

Preprints (www.preprints.org) | NOT PEER-REVIEWED | Posted: 27 February 2023 doi:10.20944/preprints202302.0431.v1

that after 4 weeks, bone defects in rat tibiae are completely filled with new bone tissue, with no inflammatory reaction [15]. The results of these investigations have shown that BNC has great potential as a bone graft and regeneration of hard tissues. But still, more research is needed to design microporous 3D scaffolds that allow cell migration and proliferation. In addition, alternatives should be sought on how to increase the bioactivity of BNC, without affecting the morphology and interconnection of the pores in the scaffolds.

The objective of this research is to design a microporous scaffold based on bacterial nanocellulose, modified through a biomineralization method of alternating cycles between calcium and phosphate solutions, in order to mimic some structural and chemical characteristics of bone tissue. As mentioned above, BNC has structural similarities to ECM of bone tissues, because its fibrils are at the nano-scale and are microscopically similar to collagen fibers [36]. In turn, the chemical characteristics of BNC (presence of OH^- groups on the surface) allow the creation of specific sites for the nucleation and growth of calcium phosphate crystals [37], through the interaction between Ca^{2+} ions and the groups OH^- of cellulose and the interaction with other ions that are naturally present in bone tissue as Na^+, Mg^{2+} and K^+ [38]. In addition, the scaffolds will be chemically characterized to establish their characteristics and similarities with native bone, and finally the results of different in vitro tests will be presented that will allow the study of cell viability and the expression of a series of specific markers that play different roles in the mesenchymal stem cell differentiation process towards an osteoblastic phenotype.

2. Materials and Methods

Scaffold Preparation

Bacterial nanocellulose (BNC) scaffolds were obtained through the fermentation of the bacterium *Komagataeibacter medellinensis* NBRC 3288 [39]. The strain was isolated at the Central Minorista de Medellín and was identified at the Universidad Pontificia Bolivariana [40]. The process of preparing the microporous 3D scaffolds was described in previous studies [41]. Briefly, nanocellulose scaffolds were prepared using a Hestrin-Schramm (HS) culture medium modified with 2% glucose (w/v), 0.5% peptone (w/v), 0.5% yeast (w/v) , disodium phosphate 0.267% (w/v) and citric acid to adjust the pH to 3.5. The medium was inoculated with 0.2 mg/l of a preinoculum of the bacterium *K. medellinensis*. Fermentation was carried out initially for 3 days under static conditions to form a thin membrane that served as a scaffold for the paraffin microspheres. After this time, 0.2 g of paraffin microparticles were added to each well, which were prepared following the method reported by Osorio et al. [42] with a size between 50 and 350 µm. The fermentation was left for 7 more days, until the nanocellulose covered the added paraffin microparticles. Then, the BNC scaffolds were purified in a 5% (w/v) KOH solution for 10 hours at 100 RPM to remove biomass and debris. The scaffolds were then washed with distilled water until neutral pH was reached. Figure 1 shows a schematic illustration of the manufacturing process of the microporous 3D scaffolds of BNC.

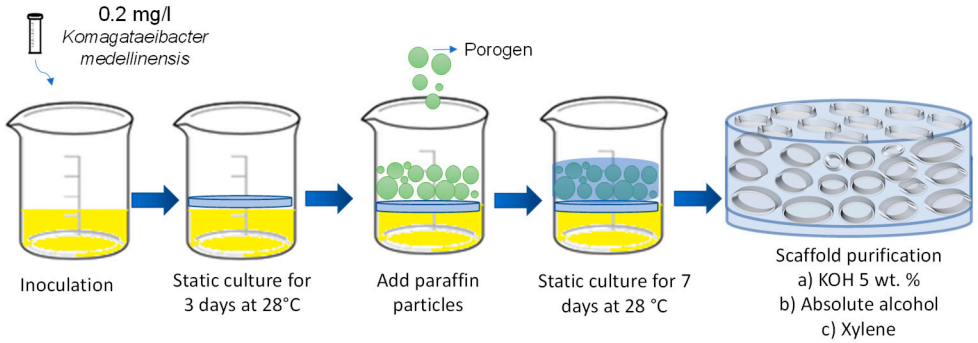

Figure 1. Schematic illustration for the design of microporous 3D scaffolds of bacterial nanocellulose.

 doi:10.20944/preprints202302.0431.v1

To eliminate the paraffin microspheres and obtain open pores, the BNC scaffolds were subjected to a series of washes with hydro-alcoholic solutions of different concentrations (40, 60, and 100% (v/v)) at intervals of 2 hours. and at 75 °C. Afterwards, they were washed with xylene 2 times for 60 minutes each wash and finally another series of washes was carried out with hydro-alcoholic solutions (100, 80, and 40% (v/v)). For all washes, a ratio of 20 g of wet BNC per 100 ml of solution was maintained. As a control, a cellulose membrane cultured for 7 days without the addition of paraffin particles was used.

Modification of the Scaffolds

This modification was carried out using cycles of two consecutive treatments. In the first treatment, the microporous 3D scaffolds of BNC were immersed in a supersaturated solution of calcium chloride ($CaCl_2$) at a pH = 7 for 48 hours. Then the scaffolds were treated with disodium phosphate solutions (Na_2HPO_4), for 48 hours. Throughout the time, the biomaterials were under dynamic conditions in an orbital shaker at 200 RPM and 37 ° C. In the first treatment, the nucleation sites for the growth of calcium phosphate crystals were generated. Materials were prepared with 1, 2, 3, 4 and 5 cycles, designated as BNC CaP-X, where X corresponds to the number of cycles. The analyzes to determine the time required for calcium adsorption on the BNC surface are reported in previous studies [41].

Characterization of the Scaffolds

The morphology and microstructure of the microporous 3D scaffolds of BNC, with and without biomineralization process, were studied by means of scanning electron microscopy (SEM), using a JEOL JSM 6490 LV equipment in high vacuum with secondary electron detector to obtain images of high-resolution SEI at an acceleration voltage 20 KV and with EDS system. The cross section of the scaffolds was coated with a thin layer of gold. The pore size of the scaffolds was measured using the free distribution software: Image J. In total, 100 surface pores were measured, taken from the SEM micrographs.

To determine the thermal decomposition of BNC and the relative proportions of the amount of mineral deposited on the surface of the material by the different treatment cycles, a thermogravimetric analysis (TGA) was performed on a Mettler Toledo TGA/SDTA 851E thermogravimetric analyzer. The samples were left to dry in a forced convection oven at 105 °C until constant weight to have a humidity control, considering the method described in T 210 cm-03 Sampling and testing wood pulp shipments for moisture. A total of 11 mg of each dry sample was used. The samples were heated from 30 to 800 °C with a heating rate of 10 °C · min-1 in a nitrogen atmosphere.

The chemical composition of the biomineralized BNC microporous 3D scaffolds was analyzed by energy dispersion X-ray spectroscopy (EDS) and by X-ray fluorescence (XRF) on the surface of each dry scaffold. For the XRF, a Thermo Scientific ARLTM Optim'x WDXDR Spectrometer was used in a helium atmosphere. In EDS analyzes, chemical compositions for all scaffolds were analyzed using X-ray elemental maps in scan mode.

To determine the presence of the functional groups of the mineral and organic phases present in the biomineralized scaffolds, Fourier transform infrared spectroscopy (FTIR) was used in attenuated total reflection (ATR) mode, using a Thermo Scientific Nicolet 6700 spectrometer. Spectra were recorded in the region between 4000–400 cm^{-1} using 64 scans and a spectral resolution of 6 cm-1. Three measurements were made on each side of the scaffolds and the spectra were averaged using the Omnic program.

By means of X-ray diffraction (XRD), the crystalline phases and the apparent crystal size of the mineral portion deposited on the scaffolds were determined. The analysis was performed using a Rigaku diffractometer with a copper (Cu) source. The diffractograms were obtained in the angular range of 5-50° with a step size of 0.02°. The data were analyzed using the software HighScore Plus Release: Version 3.0d, to determine the crystalline phases of the biomineralized portion present in

 doi:10.20944/preprints202302.0431.v1

each modified scaffold through the Search and Match function [43,44]. The apparent crystal size (τ) was found using the Scherrer Equation (1) [4]:

$$\boldsymbol{\tau = K\lambda/\beta cos\theta} \quad (1)$$

where K is a shape factor, for which a value of 0.94 was chosen which is used for elongated bone crystallites [4] λ is the wavelength of X-rays (0.15406 nm), θ is the Bragg angle and β is the width at mean height (FWHM) of the maximum intensity corresponding to the reflection of the (002) plane [44,45].

Cells Studies

In vitro biological assays were performed with human bone marrow mesenchymal stem cells (BM-MSC), which were isolated from a bone marrow biopsy to obtain a primary cell culture. Signed informed consent was provided by healthy donors. Cells were cultured with Dulbecco's Modified Eagle's culture medium (DMEM) media, with 10% FBS, 100 U/ml penicillin and 100 µg/ml streptomycin at 37ºC, under 5% CO_2. The BNC holders were sterilized in a LabTech autoclave for 20 minutes at 121 °C. Then, the materials were washed twice with a sterile phosphate buffer solution (PBS) and finally, a wash with DMEM was performed.

The number of viable cells in direct contact with the scaffolds was determined by the formation of a colored compound, due to a reaction that takes place in the mitochondria of viable cells with the bromide of 3-(4, 5-dimethylthiazol-2- yl) -2,5-diphenyl-2H-tetrazol-3-io (MTT). To obtain these results, the cells were first seeded in 96-well plates with a density of 4.0×10^3, 5.0×10^3 and 6.0×10^3 cells/well for specific time points of 24, 48 and 72 hours. Then, 0.1 g/ml of the BNC scaffolds were incubated as previously mentioned, for the established times and following the international standard ISO 10993-5 2009. After each incubation period, the scaffolds were carefully removed, the culture medium was removed and 90 µL of fresh complete medium, plus 20 µl of 5 mg/ml MTT (Cayman Chemical, Ann Arbor MI, USA) were added per well and incubated for 4 hours at 37 ° C. Then the media was removed and 100 µl well of dimethylsulfoxide (DMSO) was added and the mixture followed by 30 minutes of constant agitation to dissolve the formazan crystals. Hydrogen peroxide was used as a positive control of 100% toxicity and wells with cells cultured without any material were used as a negative control. The test was carried out in triplicates.

The secretion activity of the enzyme alkaline phosphatase (ALP) was determined using the Alkaline Phosphatase Detection kit, fluorescence (APF-1KT) (Sigma-Aldrich). The scaffolds were placed in 96-well culture dishes, 200 µl of DMEM medium with a density of 10x103 cells/well was added, they were incubated for 7 and 14 days at 37 °C in a humid atmosphere and 5% CO_2. The culture media were conditioned to compensate for the loss of evaporated water in the dishes due to the incubation time. After each time, 180 µl of the solution prepared with the kit was added to each well. The absorbance was measured at a wavelength of 440 nm using a microplate reader (Bio-Rad). This assay was performed in triplicate and a fibroblast culture was used as a negative control and BM-MSC cells as a positive control to determine the basal level of ALP.

The expression of the osteopontin (OP) and osteocalcin (OC) was identified through the Western Blot technique. To carry out this assay, an in vitro culture of BM-MSCs was first performed on the scaffolds in the same way as explained above. After 21 days, the culture medium was removed from the wells and the cells were detached from the scaffolds with a trypsin solution. The solutions with the cells were centrifuged at 5000 RPM for 5 minutes at 4 °C. The cells obtained were lysed to release the proteins, using a RIPA buffer (20-188, Sigma) supplemented with protease and phosphatase inhibitors. Total protein content was determined using a BCA protein assay kit (23225, Thermo Fisher). Once the proteins obtained in each culture had been quantified on the BNC scaffolds, 10 µg were loaded and separated in acrylamide gels at 14% (w/v) acrylamide. gels were mounted in an electrophoresis chamber at 180 V for 2 hours at room temperature.

Then, the gel proteins were transferred to nitrocellulose membranes and placed in a chamber applying a voltage of 40 V for 2 hours at 4 °C. The membrane was then incubated for 2 hours in a blocking buffer in a phosphate buffer solution with 4% (w/v) Tween 20 (PBST). The membranes were

 doi:10.20944/preprints202302.0431.v1

then incubated with the primary antibodies (osteopontin AB10910 and osteocalcin AB 10911 Millipore) at a final concentration of 1 μg / ml in phosphate buffer-Tween 20 (PBST) for 12 hours at 4 °C. After this time, the membranes were incubated for 1 hour at room temperature with a secondary antibody IgG-HRP (AP160P, Millipore) at a final concentration of 1 mg/ml in PBST. Finally, the membranes were reveled on a Luminata ™ Forte Western HRP transilluminator (WBLUF0100, Millipore). The culture of the unmodified BNC scaffolds was used as a positive control, in a culture medium StemPro ™ Osteogenesis Differentiation Kit, which allows the complete differentiation of human mesenchymal stem cells into bone cells. Unmodified BNC scaffolds were used as negative control in DMEM culture medium. These tests were carried out at the Ramon Llull University, Barcelona-Spain

Finally, for all the tests that required it, statistical analyses were carried out using the Statgraphics Centurion Version 2007. The data were analyzed by analysis of variance (ANOVA) and the differences between the means determined by the LSD Fisher multiple comparison test. For data of test pairs that did not meet the assumptions for ANOVA, were performed a Kruskal–Wallis (K–W) test. A value of $p \leq 0.05$ was considered statistically significant.

3. Results and Discussion

The characteristics of the scaffolds were determined through different physical and chemical analysis. Figure 2 shows the photographs and electron microphotographs of the BNC membrane used as a control (Figure 2a,c) and the microporous 3D BNC scaffold (Figure 2b,d). In the photograph of Figure 2-a it can be seen that the surface of the nanocellulose membrane used as a control is more compact, compared to the surface of the microporous material, which shows a greater roughness associated with the paraffin particles (see Figure 2b). The electron micrographs show that the BNC scaffolds that were obtained with the paraffin particles have a large number of pores, with a homogeneous distribution and a high interconnection between them (see Figure 2d). The pore size distribution is between 70 and 350 μm. The pores maintained the spherical shape of the paraffin particles, suggesting that the process used to remove the paraffin from the BNC scaffolds is not aggressive and does not alter the 3D structure of the material. The results obtained up to this point are promising, since one of the key elements in bone tissue engineering is to manufacture a 3D scaffold with a porous and interconnected structure to subsequently allow cell migration and proliferation [23,27]. Some research assures that a pore size of 100 μm allows cell migration, since the small pores favor hypoxic conditions and osteochondral formation. Other research assures that pore sizes of around 300 μm easily allow revascularization, which favors osteogenesis, but the functional limit for pore size and their distribution has not yet been established, in order to regenerate the bone properly [46,47]. Some studies have shown that porosity is a key characteristic of bone grafts, since a high percentage of porosity and also interconnected between 100 and 500 μm is important for vascularization and can serve as a scaffold for osteoconductivity [45]. Therefore, it can be concluded that the pore size distribution obtained in the designed scaffolds will help the formation of the new tissue.

Preprints (www.preprints.org) | NOT PEER-REVIEWED | Posted: 27 February 2023 doi:10.20944/preprints202302.0431.v1

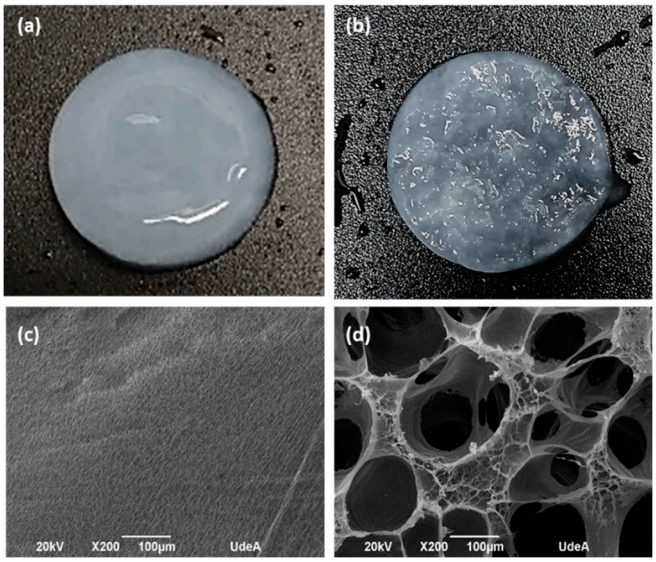

Figure 2. Scaffold morphologies a) photograph and c) micrograph taken by SEM of BNC membrane used as control; b) photograph and d) micrograph taken by SEM of microporous 3D BNC scaffold.

In Figure 3, the microporous 3D scaffolds of BNC can be observed after the biomineralization cycles (BNC CaP-1 to BNC CaP-5). In the 200x micrographs, it can be seen that crystals are formed along the entire surface of the BNC pores and that the number and size of the crystals increase with increasing number of cycles. The growth of crystals around cellulose nanofibers are shaped like bars or needles as reported by other authors [15,48]. In the 5,000x micrographs, it is observed that as the number of cycles increased, the distribution of the crystals was more homogeneous throughout the surface, and larger crystallites were formed as reported by other authors [48,49]. In the 200x micrographs, it is observed that until cycle 3, the surface of the BNC is completely covered by the calcium phosphate crystals, but the interconnectivity between the pores is still preserved (see Figure 3, BNC CaP-3 column), while from the 4th and 5th cycle of the treatment, the crystals increased in size and quantity, closing the pores (see Figure 3 column BNC CaP-4 and BNC CaP-5). Closed pores are not suitable from the point of tissue engineering since, as mentioned, scaffolds designed for tissue regeneration must have a network of interconnected pores to allow cell migration, revascularization and the transport of nutrients to the cells.

In the lower part of Figure 3, the homogeneous distribution of calcium and phosphate ions along the surface of the BNC from cycle 1 to cycle 5 can be observed in the elemental maps taken with the EDS. The results obtained suggest that cyclical treatments with saturated CaCl2 solutions followed by Na2HPO4 solutions, under dynamic conditions, permitted to simulate the mineralization conditions of bone tissues. Zimmermann, et al. (2011), with this particular method, demonstrated that pretreatment with calcium allowed the creation of a nucleation site for the growth of the calcium phosphate crystal [50].

Preprints (www.preprints.org) | NOT PEER-REVIEWED | Posted: 27 February 2023 doi:10.20944/preprints202302.0431.v1

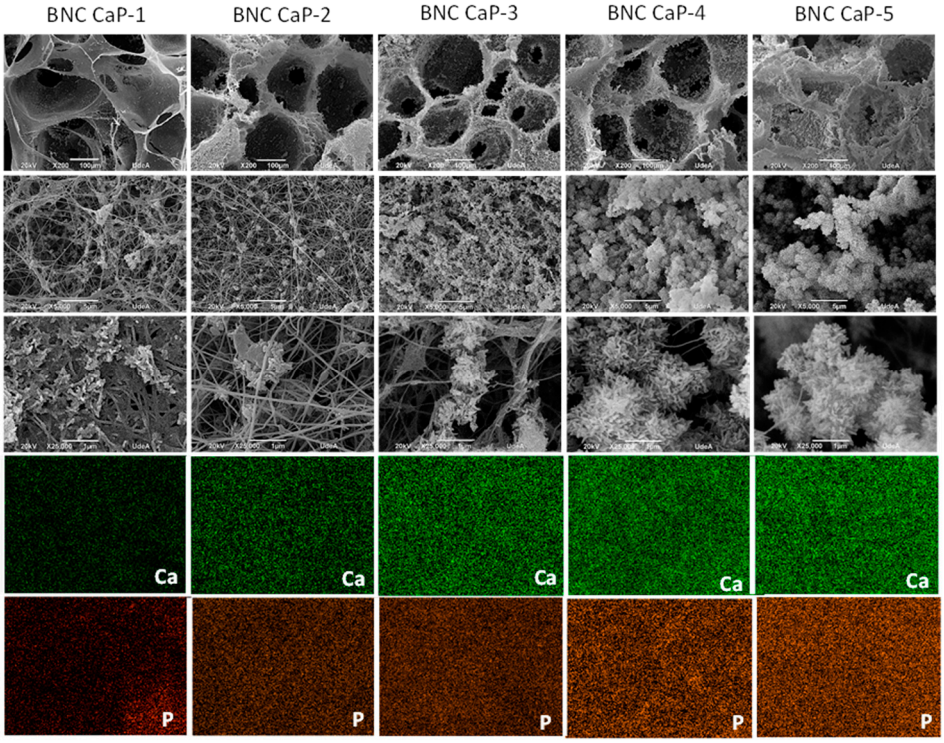

Figure 3. Electron micrographs taken by SEM at 200x, 5000x and 25000x (rows 1 to 3) and elemental maps made by EDS with a scale of 10 µm (rows 4 and 5) of the microporous 3D scaffolds of biomineralized BNC. From left to right column 1: BNC control, column 2: BNC cycle 1, column 3: BNC cycle 2, column 4: BNC cycle 3, column 5: BNC cycle 4, and column 6: BNC cycle 5.

Figure 4 shows the thermograms obtained for the different materials. The results show that as the number of biomineralization cycles increases, the amount of mineral precipitated on the surface of the BNC scaffolds also increases. The percentage of solid waste by mass after 800 ° C increased as follows: 34.8% for cycle 1; 48.8% for cycle 2; 59.6% for cycle 3; 64.6% for cycle 4, and 67.8% for cycle 5. This increase is associated with the greater precipitation of calcium and phosphate ions with the increase of the treatment cycles, as also reported by Hutchens et al. (2006) [48], and as corroborated with the electron microscopies of Figure 3, where the size and quantity of the crystals increase with the increase in the number of cycles. The mass loss rate of BNC was 11.3% due to charred ash in the nitrogen atmosphere [51].

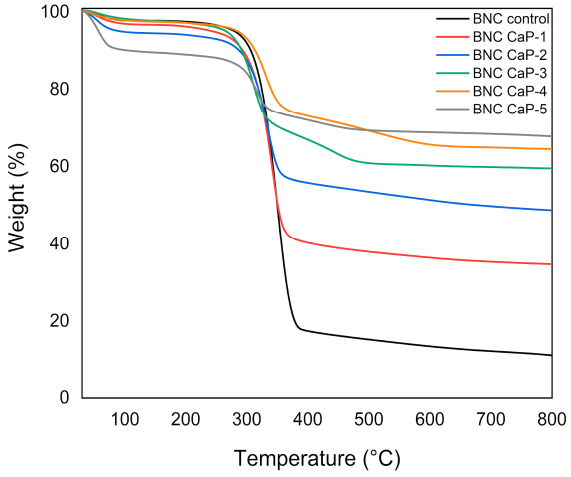

Figure 4. Results of thermogravimetric analysis of biomineralized BNC microporous 3D scaffolds. An unmodified BNC microporous 3D scaffold was used as a control.

Table 1 shows the results obtained in the mass fraction (% by weight) per chemical element by XRF. There it is observed that after the biomineralization cycles, the Ca and P elements are the ones that were found in the highest percentage on the surface of the BNC, followed by the Na element. Calcium is the element with the highest concentration in all scaffolds, because the hydroxyl groups on the surface of cellulose created a negatively charged surface at pH ~ 7.0, which allows the interaction of calcium ions between the functional groups by electrostatic interactions. In addition, all hydroxyl groups in cellulose have negative dipoles that could chelate calcium ions ($Ca^{2+)}$ in solution and form a coordinated bond [41].

Table 1. Results of the elemental analysis by X-ray fluorescence.

Scaffold *	Ca	P	Na	Mg	S	K	Cl	Fe	Si	CaO	P_2O_5	Ca/P (atomic %)
NCB CaP-1	10.33	7.09	1.01	-	0.03	0.01	0.10	0.02	-	19.34	20.01	1.13
NCB CaP-2	16.90	10.94	1.11	-	0.45	0.07	0.20	0.04	-	23.64	23.69	1.19
NCB CaP-3	20.74	12.95	0.68	-	0.03	0.01	0.07	0.03	-	29.01	29.67	1.24
NCB CaP-4	22.16	14.01	1.22	-	0.03	0.01	0.05	0.03	0.01	31.00	32.10	1.22
NCB CaP-5	26.61	12.82	0.82	-	0.02	0.02	0.16	0.04	0.03	37.22	29.83	1.60

* One gram of sample (% mass), of the microporous 3D scaffolds of biomineralized BNC and the Ca/P ratio atomic %.

The results showed that the calcium phosphate ratio (Ca/P) increases with the increase in the number of cycles in the treatment. Even so, this ratio in all biomineralized scaffolds is lower than that of stoichiometric hydroxyapatite (HA), which reports a Ca/P 1.67 ratio. Hydroxyapatite is one of the most used bone grafts, but in general the Ca/P ratio of the bone increases with the age of the individuals and bone maturation as confirmed by some reports in the literature [4,52]. This represents an advantage of the biomaterials designed in this work, since it shows that synthetic bone grafts can be manufactured with Ca/P ratios similar to natural bone and taking into account the compositional variation of this tissue, which is associated with formation rates and bone resorption during the remodeling process, and where Ca is found in greater quantity throughout the surface, since this ion plays a very important role in the formation of HA crystals in new bone [52]. Furthermore, Na^{2+} also plays an important role in bone crystal formation, as it often tends to replace Ca^{2+} in the crystal lattice of biological hydroxyapatite [38,52]. In addition to this, in Table 1 it can be seen that oxides such as CaO, P_2O_5 were found, which are characteristic for the bone mineral.

In Figure 5, the infrared spectrum of the microporous 3D scaffolds of biomineralized BNC are observed with respect to the control BNC. The characteristic bands of the BNC are found at ~3350 cm^{-1} which is attributed to the stretching vibrations of the –OH group. The bands at ~2890 cm^{-1}, ~1645 cm^{-1}, ~1440 cm^{-1} and ~1065 cm^{-1}, are attributed to stretching vibrations of C – H and $–CH_2$, the bending of –OH from adsorbed water, the symmetric bending of $–CH_2$ and the skeletal vibrations of the pyranose ring C – O – C, respectively [53]. The bands at ~1370 cm^{-1}, ~1340 cm^{-1} and ~1315 cm^{-1}, are attributed to the bending of –CH, the bending in the –OH plane, and the undulation of $–CH_2$. This indicates the presence of crystalline regions within the structure of the BNC. Finally, the bands at ~750 cm^{-1} and ~710 cm^{-1} are related to the presence of crystalline Iα and Iβ allomorphisms of cellulose [47]

In Figure 5 it can also be observed that as the number of biomineralization cycles of the scaffolds increases, the band ~3350 cm^{-1} attributed to the BNC begins to disappear due to the cellulose being covered (Fig 5 green region) as reported by other authors [37,54] and the $u_3PO_4^{3-}$ band appears more defined and with greater intensity at ~1200-900 cm^{-1} (indicated in the blue region of Figure 5), which is associated with calcium phosphates. This band becomes more defined, and narrower as the number of cycles increases. The narrowness of this band is associated with the crystallinity of calcium phosphates [54,55]. In other words, the amount and crystallinity of the calcium phosphates precipitated on the BNC increases with the increase in the number of cycles. As the number of cycles

Preprints (www.preprints.org) | NOT PEER-REVIEWED | Posted: 27 February 2023 doi:10.20944/preprints202302.0431.v1

increase, other characteristic bands also appear, such as $u_3PO_4^{3-}$ associated with phosphate ions that resolve into two peaks around 650-500 cm^{-1} [55,56] (marked in the blue region). The presence of this shoulder becomes more evident from cycle 2 to cycle 5 (BNC CaP 2-5), and as reported in the literature, this may be indicative that an octacalcium phosphate (OCP) is being formed, which it is the precursor phase in the formation of HA. As explained by Hutchens, et al. (2006), the hydroxyl groups of cellulose have a strong negative dipole that could chelate the free Ca^{2+} cations in the $CaCl_2$ solution and form a coordinate bond or have an ion-dipole interaction. The phosphate ions can then bind with calcium already associated with cellulose to form calcium phosphate. Therefore, there is no direct initial interaction between calcium and phosphate, but first the calcium ions are ordered on the BNC before mineralization, obtaining a phase not as crystalline as the OCP, but with the increase of the number of cycles ensures a more crystalline and ordered apatite phase [48].

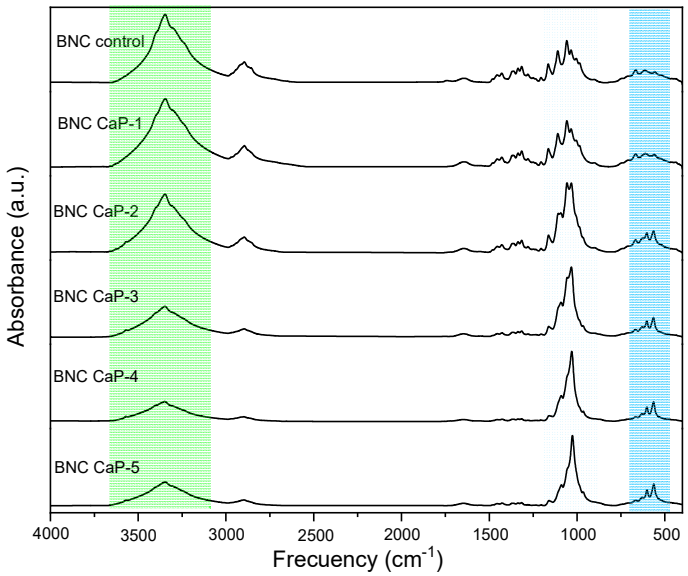

Figure 5. Analysis of the spectra obtained by FTIR-ATR of the microporous 3D scaffolds of biomineralized BNC.

Figure 6 shows the diffractograms obtained from the microporous 3D scaffolds of biomineralized BNCs. All the scaffolds designed showed the three characteristic cellulose peaks assigned to the crystallographic planes (1 0 0), (0 1 0), and (1 1 0), which correspond to the diffraction angles of 14.6 °, 16.8 ° and 22.8 °, respectively. In the blue region indicated in Figure 6, it is observed that as the amount of minerals deposited on the surface of the scaffolds increases, the intensity of the BNC peaks decreases. The decrease in the intensity of these peaks shows that as the microporous 3D scaffolds are modified with the biomineralization treatment, the mineral phases become the dominant component of the scaffold due to the increase in the amount of calcium phosphates, such as this is also confirmed by studies carried out by Hutchens et al. (2006) and Yin et al. (2011), showed in the mineralization processes carried out on cellulose membranes [48,53].

Preprints (www.preprints.org) | NOT PEER-REVIEWED | Posted: 27 February 2023 doi:10.20944/preprints202302.0431.v1

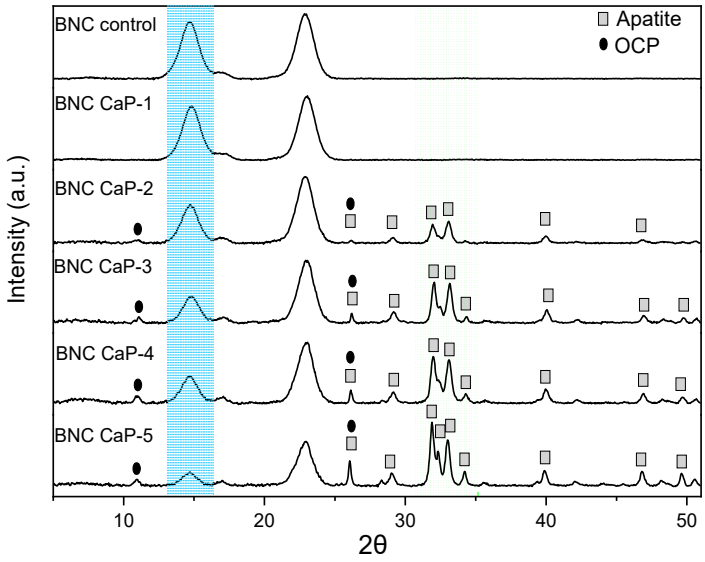

Figure 6. Phase analysis of the diffractograms of the biomineralized NCB microporous 3D scaffolds.

Therefore, for the semi-quantitative phase analysis through the HighScore software, the mineral elements found by XRF were used as established restrictions and the characteristic peaks of cellulose were eliminated. In the phase analysis of the microporous 3D scaffolds of BNC, it was found that in the treatment with one cycle no characteristic mineral phase is still observed, and only from the treatments with 2 cycles and up to 4 cycles, the phases are found of octacalcium di-hydrogen phosphate pentahydrate (OCP) and apatite-(CaOH). In cycle 5, the percentage of the apatite phase was predominant (see green region of Figure 6). Table 2 shows the semi-quantitative results obtained in the HighScore.

Table 2. Results of semi-quantitative mineral phase analyzes performed on HighScore Plus Release Software: Version 3.0 d.

Scaffold	Phase	Semiquantitative %
NCB CaP-1	Calcium	98
NCB CaP-2	Calcium	14
	Apatite	28
	OCP	58
NCB CaP-3	Calcium	8
	Apatite	22
	OCP	71
NCB CaP-4	Calcium	8
	Apatite	24
	OCP	78
NCB CaP-5	Calcium	5
	Apatite	95

This information is correlated with the diffractograms of Figure 6, where it can be observed that there is an increase in the crystalline peaks associated with the OCP and apatite phases found in the biomineralized scaffolds from cycle 2. The main diffracted peaks of the phase of apatite on the scaffolds are 25.86 °, 28.73 °, 31.7 °, 32.14 °, 32.8 °, 34.01 °, 39.67 °, 46.57 ° and 49.41 °, which correspond

 doi:10.20944/preprints202302.0431.v1

respectively to the diffraction planes (0 0 2), (1 0 2), (2 1 1), (1 1 2), (3 0 0), (2 0 2), (3 1 0), (2 2 2) and (2 1 3) [44,57]. The diffracted peaks for the phase on the OCP scaffolds were found at 26.37 ° and 32.56 ° that correspond to the diffraction planes (0 0 2) and (7 0 0) respectively [58], and they are more evident in the BNC scaffolds from the third treatment cycle. These mineral phases correspond to the Ca/P ratios found in the materials by XRF, which are between 1.19 and 1.60. These two phases of calcium phosphates are predominant in human bones, which shows us that this biomeralization method allows us to design materials with great similarity to the mineral phases of the bone.

Finally, the microporous 3D scaffolds of biomineralized BNCs showed from the second cyclic treatment the presence of the crystallographic plane at (0 0 2) which corresponds to the diffraction angle at 26.3 °, which is associated with both the apatite phase as to the OCP phase. From the width at the mean height (FWHM) of the maximum intensity corresponding to the reflection of the plane (0 0 2), the apparent size of the crystal of the different biomineralized scaffolds can be determined [31,44,45]. Table 3 shows the values of the apparent crystal size of the biomineralized scaffolds from the second to the fifth cycle. The results show that as the number of cycles in the biomimetic treatment increases, the apparent size of the crystal increases. The apparent size of the crystals found in these scaffolds is within the range of the sizes reported in the literature [48,54]. These results are consistent with what is observed in the micrographs in Figure 3, where larger crystals are formed as the number of cycles increases.

Table 3. Results of the apparent size of the crystal in the plane (0 0 2), of the 3D microporous scaffolds of BNC.

	Apparent crystal size in the crystallographic plane (0 0 2)		
Scaffold	**2θ**	**(τ) nm**	**d (nm)**
BNC CaP 2	26.15	25.12	0.34
BNC CaP 3	26.21	34.70	0.34
BNC CaP 4	26.14	36.12	0.34
BNC CaP 5	26.06	35.90	0.34
HA *	25.81	54.36	0.34

* Commercial hydroxyapatite taken as reference.

Cells Studies

The *in vitro* behavior of the scaffolds was determined by cytotoxicity tests and APL, OP and OC protein expression in BM-MSC cells, which are well described as precursor cells of obteoblasts [11]. Figure 7 shows the results obtained by the MTT assay after 24, 48 and 72 hours of BM-MSC cells culture. During the firsts 24 and 48 hours, cell viability remained 100% and no statistically significant differences ($P > 0.05$) were observed between the different designed BNC scaffolds and the unmodified BNC used as control (see the red dotted line in Figure 7). After 72 hours of culture, however, all the designed scaffolds presented a statistically significant difference ($P < 0.05$) in the percentage of cell viability, with respect to the culture after 24 hours. But cell viability remained above 90% for all scaffolds. The decrease in the percentage of cell viability at 72 hours could be explained by the increase in Ca^{2+} concentrations in the culture medium, released by the scaffolds that were

Preprints (www.preprints.org) | NOT PEER-REVIEWED | Posted: 27 February 2023 doi:10.20944/preprints202302.0431.v1

initially treated with super-saturated calcium solutions. As reported by Lee et al. (2018), adequate Ca^{2+} concentrations in the culture medium improve cell adhesion, proliferation and differentiation, but if they are very high in the assay microenvironment (culture dishes) they can be toxic to cells [59]. Therefore, future research requires a study of the microenvironment generated by biomineralized BNC scaffolds and whether or not there is release of ions associated with calcium phosphate crystals in the culture medium over time.

Another important factor to consider is the depletion of nutrients in the growing medium over time. The designed scaffolds, being microporous, have a much greater surface area than the flat surface of the culture dish, used as a negative control. Therefore, there is a considerable initial increase in cell density, as can be seen in Figure 7, where viability is higher than the negative control (red dotted line), after 24 hours and in most cases it is maintained after 48 hours. In general, these cell viability results suggest that the protocols designed for the preparation of the microporous 3D scaffolds, the washes to remove the porogenic agents from paraffin, the biomineralization methods and the nature of the materials do not generate any cytotoxic damage to the cells and on the contrary allow a viable and proliferating cell culture.

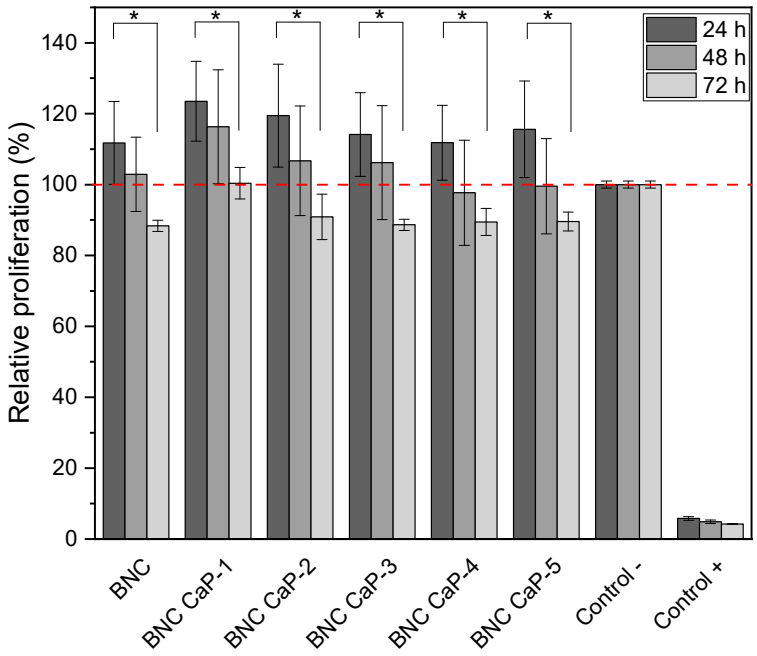

Figure 7. Viability of BM-MSC cultured on biomineralized BNC microporous scaffolds. Hydrogen peroxide was used as positive control and cells grown in the dish were used as negative control. * Significant difference ($P < 0.05$) at a confidence level of 95% (n=3). Data were analyzed by one-way ANOVA test.

Figure 8 shows the expression of ALP after 7 and 14 days for each of the designed BNC scaffolds, including the unmodified BNC and the controls. Alkaline phosphatase (APL) plays an important role in the bone mineralization process and it is used as an early marker in the differentiation of BM-MSC towards osteoblasts (Sharma et al. 2014). After 7 days of culture, a statistically significant difference ($P < 0.05$) in ALP expression was observed between BM-MSC cells incubated with BNC scaffolds and control cells (see blue asterisks). All cells incubated with BNC scaffolds express a higher level of ALP (blue dotted line). BM-MSCs were used to analyze the basal level of ALP from cells without stimulation. ALP expression did not show statistically significant differences ($P > 0.05$), between BM-MSC cultured on the plate, with respect to BM-MSC cultured on BNC scaffolds without any biomineralization treatment. As reported by Shi et al. (2012), BNC alone does not favor the expression of ALP in amounts comparable to the baseline level of MSCs [60].

Preprints (www.preprints.org) | NOT PEER-REVIEWED | Posted: 27 February 2023 doi:10.20944/preprints202302.0431.v1

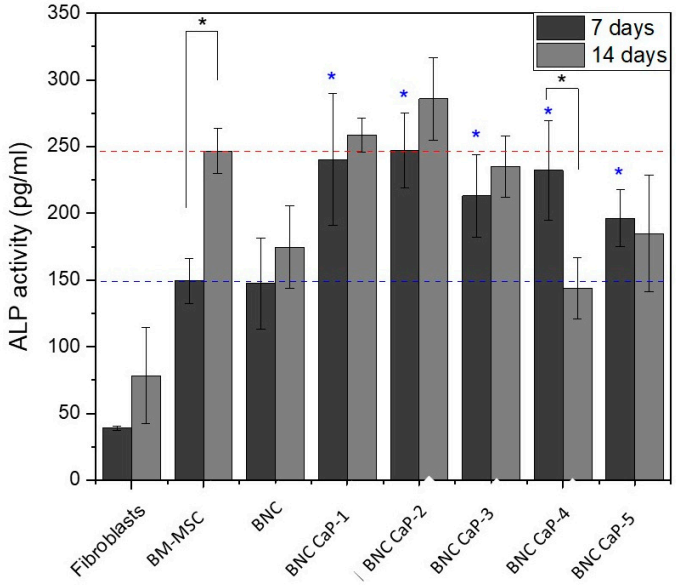

Figure 8. Expression of ALP in BM-MSC cultured on biomineralized BNC microporous scaffolds for 7 and 14 days. A culture of fibroblasts, which are cells that do not express ALP, was used as negative control, and BM-MSC cells were used as positive control to determine the basal level of ALP. * Significant difference ($P < 0.05$) at a confidence level of 95% (n=3). Data were analyzed by the Kruskal-Wallis test.

On the other hand, after 14 days of culture, a higher expression of ALP activity was obtained only in the BNC CaP-1, BNC CaP-2 and BNC CaP-3 scaffolds compared to the basal level of BM-MSC. In the other BNC scaffolds, a decrease in ALP is observed comparing between 7 and 14 days of culture. An explanation for the decrease in ALP is based on the fact that the increase in this enzyme during the first 7 days is an indicator that there is an active differentiation process of BM-MSC towards pre-osteoblasts [11,61], allowing the creation of nucleation sites for mineralization of bone tissue. Then, as reported by various authors, after the start of mineralization, ALP is no longer needed and therefore the cellular levels of the enzyme decrease before a mature mineralized matrix is formed. Therefore, the decrease in the expression of ALP may be indicative of the initiation of biomineralization of pre-osteoblasts on the designed BNC scaffolds [62,63]. The results of ALP expression of BM-MSC grown on the different biomineralized BNC scaffolds show us that biomineralized BNC scaffolds do promote the secretion of this protein by BM-MSC.

Finally, the expression of osteopontin (OP) and osteocalcin (OC) was determined in order to follow the different stages in the process of cellular differentiation of BM-MSC towards osteoblasts. Figure 9 shows the results obtained by Western blot of the expression of the OP and the OC of the BM-MSC grown on the microporous scaffolds of biomineralized BNC after 21 days of culture. In all the scaffolds it is observed that there is an expression of OP with three bands, where the thickest and most intense band is around 60 kDa (molecular weight associated with the characteristics of the primary antibody used). An increase in the intensity of OP expression was also observed as the number of cycles increased. The BNC scaffold without any biomineralization process shows OP expression with a very low intensity compared to the biomineralized BNC scaffolds. As mentioned above, the BNC CaP-4 and BNC CaP-5 scaffolds showed a decrease in ALP after 14 days of culture as shown in Figure 8. Uniting both results, it can be interpreted that these treatments may have accelerated the maturation process of the pre-osteoblasts towards the osteoblasts. In general, the expression of OP in all biomineralized BNC scaffolds indicates that there is a maturation process of pre-osteoblasts towards osteoblasts [59], compared with the positive control (which consisted of the culture of BM-MSC on unmodified BNC scaffolds, in a culture medium that allows complete differentiation of human mesenchymal stem cells into bone cells) and the negative control. This result

Preprints (www.preprints.org) | NOT PEER-REVIEWED | Posted: 27 February 2023 doi:10.20944/preprints202302.0431.v1

also suggests that the designed scaffolds have a high osteoinductive potential, since during the process of new bone formation, this protein adheres to the surface of the mineralized material helping to activate the cellular signaling pathways to attract the progenitor cells of osteoblasts and the regulation of mineralization by improving the material-new bone interface [64]. In addition, by containing RGD (arginine-glycine-aspartic acid) domains in its amino acid sequence, the presence of this protein improves cell adhesion, promotes bone formation through intra and extracellular regulation of Ca^{2+} and bone resorption. by having chemotactic activity for osteoclasts [59,65].

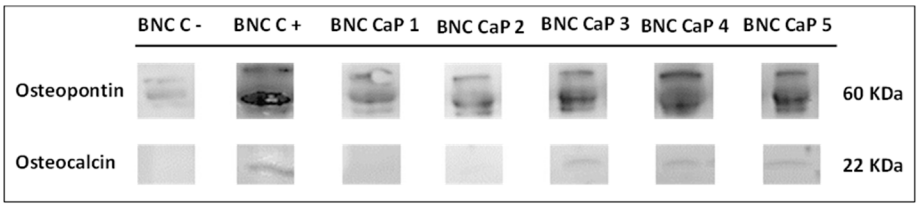

Figure 9. Expression of OP and OC of BM-MSC cultured on biomineralized BNC microporous scaffolds after 21 days of culture. As a positive control, the culture of the unmodified BNC scaffolds was used, in a culture medium that allows the complete differentiation of human mesenchymal stem cells in bone cells. Unmodified BNC scaffolds in DMEM culture medium were used as negative control.

On the other hand, Figure 9 also shows that after 21 days of culture, the OC protein is expressed around 22 kDa only on the BNC CaP 3, BNC CaP 4 and BNC CaP 5 scaffolds. OC is a specific protein in bones synthesized only by mature osteoblasts and involved with the binding of calcium and hydroxyapatite [11,66]. Therefore, the presence of this protein in the BM-MSC cultures on the aforementioned scaffolds, suggests that these materials favored osteoblastic differentiation [67,68] after 21 days of culture, compared to the other BNC scaffolds.

4. Conclusions

The results obtained show that as the number of cycles in supersaturated solutions increases, the amount of minerals mentioned above increases and the amount and size of calcium phosphate crystals on the surface of the microporous 3D BNC scaffolds increases. This affected the size and interconnection between the pores, which could hamper the tissue formation process. For this reason, it is advisable to carry out a biomineralization treatment of up to 3 cycles.

In vitro cultures demonstrated that the materials and processes designed to manufacture the three-dimensional scaffolds do not affect cell viability. In addition, through the detection of different specific cell markers in the process of bone maturation in vivo, it was shown that the microporous 3D scaffolds of biomineralized BNCs generally favor the different differentiation stages of BM-MSC towards osteoblasts. This was demonstrated with the early expression of alkaline phosphatase (ALP), which indicates that BM-MSC differentiated into pre-osteoblasts. Then, a high expression of osteopontin (OP) was observed, which shows that the pre-osteoblast maturation process continues and marks the beginning of mineralization. The detection of the expression of osteocalcin (OC) was detected only in the BNC CaP-3 scaffolds, which is an indicator that these materials could possibly accelerate the maturation process *in vivo* and increase the degree of bone mineralization, compared to the other scaffolds who also showed to favor the differentiation process. These results are promising since the differentiation behavior of the designed BNC scaffolds is analogous to what occurs in the maturation and remodeling process of bone.

Author Contributions: Conceptualization, Ana Cañas-Gutiérrez; **methodology**, Ana Cañas-Gutiérrez, Cristina-Fornaguera, Marlon Osorio, and David Arboleda-Toro.; **validation**, Ana Cañas-Gutiérrez, Marlon Osori and Cristina Castro-Herazo; **formal analysis**, Ana Cañas-Gutiérrez, Salvador-Borrós and David Arboleda-Toro; **investigation**, Ana Cañas-Gutiérrez; **resources**, Ana Cañas-Gutiérrez, Cristina Castro-Herazo, and David Arboleda-Toro; **data curation**, Ana Cañas-Gutiérrez.; **writing—original draft preparation**, Ana Cañas-Gutiérrez.; **writing—review and editing**, Ana Cañas-Gutiérrez, Lenka Toro and David Arboleda-Toro .;

visualization, Ana Cañas-Gutiérrez. Cristina-Fornaguera, and Salvador-Borrós; **supervision**, Ana Cañas-Gutiérrez.; **project administration**, Ana Cañas-Gutiérrez.; **funding acquisition**, Ana Cañas-Gutiérrez. All authors have read and agreed to the published version of the manuscript.

Funding: This research was funded by Ministry of Science, Technology, and Innovation (Min- 433 Ciencias) , MINEDUCACIÓN, MINCIT, and ICETEX, through the Program Ecosistema Científico Cod. FP44842-211-2018 Project numbers, 58674 and FONDO FRANCISCO JOSÉ DE CALDAS grant 1210-903-86606 CT 80740-448-2021: 434 "Misión Bioeconomía para una Colombia potencia viva y diversa hacia una sociedad impulsada 435 por el conocimiento" and Centro de Investigación para el Desarrollo y la Innovación –CIDI- from 436 Universidad Pontificia Bolivariana.

Institutional Review Board Statement: Not applicable.

Informed Consent Statement: Not applicable.

Data Availability Statement: The data presented in this study are available on request from the corresponding author.

Acknowledgments: The Authors acknowledge the help of Mònica Guarro with the Western Blotting Technique.

Conflicts of Interest: The authors declare no conflict of interest.

References

1. S. Wu, X. Liu, K. W. K. Yeung, C. Liu, and X. Yang, "Biomimetic porous scaffolds for bone tissue engineering," *Materials Science and Engineering R*, vol. 80, pp. 1–36, 2014, doi: 10.1016/j.mser.2014.04.001.
2. J. Sundberg, C. Götherström, and P. Gatenholm, "Biosynthesis and in vitro evaluation of macroporous mineralized bacterial nanocellulose scaffolds for bone tissue engineering," *Biomed Mater Eng*, vol. 25, no. 1, pp. 39–52, 2015, doi: 10.3233/BME-141245.
3. A. Goharian, M. Kadir, and M. Abdullah, *Trauma Plating Systems: Biomechanical, Material, Biological, and Clinical Aspects*. Amsterdam, 2017.
4. R. Legros, N. Balmain, and G. Bonel, "Age-related changes in mineral of rat and bovine cortical bone," *Calcif Tissue Int*, vol. 41, no. 3, pp. 137–144, 1987, doi: 10.1007/BF02563793.
5. M. Bohner, "Physical and chemical aspects of calcium phosphates used in spinal surgery," *European Spine Journal*, vol. 10, no. SUPPL. 2, pp. 114–121, 2001, doi: 10.1007/s005860100276.
6. A. Boskey, "Bone mineral crystal size," vol. 14, pp. 16–21, 2003, doi: 10.1007/s00198-003-1468-2.
7. R. J. Kroeze, M. N. Helder, L. E. Govaert, and T. H. Smit, "Biodegradable polymers in bone tissue engineering," *Materials*, vol. 2, no. 3, pp. 833–856, 2009, doi: 10.3390/ma2030833.
8. K. B. S. Paiva and J. M. Granjeiro, "Bone tissue remodeling and development: Focus on matrix metalloproteinase functions," *Arch Biochem Biophys*, vol. 561, pp. 74–87, 2014, doi: 10.1016/j.abb.2014.07.034.
9. W. G. de Long *et al.*, "Bone grafts and bone graft substitutes in orthopaedic trauma surgery. A critical analysis.," *J Bone Joint Surg Am*, vol. 89, pp. 649–658, 2007, doi: 10.2106/JBJS.F.00465.
10. N. Shibuya and D. C. Jupiter, "Bone Graft Substitute: Allograft and Xenograft," *Clin Podiatr Med Surg*, vol. 32, no. 1, pp. 21–34, 2015, doi: 10.1016/j.cpm.2014.09.011.
11. R. J. Miron and Y. F. Zhang, "Osteoinduction: A review of old concepts with new standards," *J Dent Res*, vol. 91, no. 8, pp. 736–744, 2012, doi: 10.1177/0022034511435260.
12. W. Pradel and G. Lauer, "Tissue-engineered bone grafts for osteoplasty in patients with cleft alveolus," *Annals of Anatomy*, vol. 194, no. 6, pp. 545–548, 2012, doi: 10.1016/j.aanat.2012.06.002.
13. G.-Y. Cho-Lee, E.-M. García-Díez, R.-A. Nunes, C. Martí-Pagès, R. Sieira-Gil, and A. Rivera-Baró, "Review of secondary alveolar cleft repair," *Ann Maxillofac Surg*, vol. 3, no. 1, p. 46, 2013, doi: 10.4103/2231-0746.110083.
14. Y. Tokugawa, M. Kubota, M. Nishimura, N. Haruyama, and K. Igarashi, "Bone regeneration of canine artificial alveolar clefts using bone-marrow-derived mesenchymal stromal cells and β-tricalcium phosphate: A preliminary study," *Orthodontic Waves*, vol. 71, no. 2, pp. 51–58, 2012, doi: 10.1016/j.odw.2012.01.003.
15. S. Saska, H. S. Barud, A. M. M. Gaspar, R. Marchetto, S. J. L. Ribeiro, and Y. Messaddeq, "Bacterial cellulose-hydroxyapatite nanocomposites for bone regeneration," *Int J Biomater*, vol. 2011, pp. 1–8, 2011, doi: 10.1155/2011/175362.
16. J. Li, Y. Wan, L. Li, H. Liang, and J. Wang, "Preparation and characterization of 2,3-dialdehyde bacterial cellulose for potential biodegradable tissue engineering scaffolds," *Materials Science and Engineering C*, vol. 29, no. 5, pp. 1635–1642, 2009, doi: 10.1016/j.msec.2009.01.006.
17. H. G. de Oliveira Barud *et al.*, "A multipurpose natural and renewable polymer in medical applications: Bacterial cellulose," *Carbohydr Polym*, vol. 153, pp. 406–420, 2016, doi: 10.1016/j.carbpol.2016.07.059.
18. G. Fadel *et al.*, "Bacterial cellulose in biomedical applications : A review," *Int J Biol Macromol*, vol. 104, pp. 97–106, 2017, doi: 10.1016/j.ijbiomac.2017.05.171.

19. N. Eslahi, A. Mahmoodi, N. Mahmoudi, N. Zandi, and A. Simchi, "Processing and Properties of Nanofibrous Bacterial Cellulose-Containing Polymer Composites: A Review of Recent Advances for Biomedical Applications," *Polymer Reviews*, vol. 60, no. 1, pp. 144–170, 2020, doi: 10.1080/15583724.2019.1663210.
20. N. Chiaoprakobkij, N. Sanchavanakit, K. Subbalekha, P. Pavasant, and M. Phisalaphong, "Characterization and biocompatibility of bacterial cellulose/alginate composite sponges with human keratinocytes and gingival fibroblasts," *Carbohydr Polym*, vol. 85, no. 3, pp. 548–553, 2011, doi: 10.1016/j.carbpol.2011.03.011.
21. M. A. Osorio *et al.*, "Synthesis of Thermoplastic Starch-Bacterial Cellulose Nanocomposites via In situ fermentation," *Journal of brazilian chemical Society*, vol. 25, no. 9, pp. 1607–1613, 2014.
22. L. Nimeskern, H. Martinez Avila, J. Sundberg, P. Gatenholm, R. Muller, and K. S. Stok, "Mechanical evaluation of bacterial nanocellulose as an implant material for ear cartilage replacement," *J Mech Behav Biomed Mater*, vol. 22, pp. 12–21, 2013, doi: 10.1016/j.jmbbm.2013.03.005.
23. A. Bodin, S. Concaro, M. Brittberg, and P. Gatenholm, "Bacterial cellulose as a potential meniscus implant," *J Tissue Eng Regen Med*, vol. 1, no. 2001, pp. 406–408, 2007, doi: 10.1002/term.
24. D. Klemm, D. Schumann, U. Udhardt, and S. Marsch, "Bacterial synthesized cellulose: artificial blood vessels for microsurgery," *Prog Polym Sci*, vol. 26, pp. 1561–1603, 2001, doi: 10.1016/S0079-6700(01)00021-1.
25. A. J. Novaes and AB. Novaes, "Bone formation over a TiAl6V4 (IMZ) implant placed into an extraction socket in association with membrane therapy (Gengiflex)," *Clin Oral Implants Res*, vol. 4, pp. 106–110, 1993.
26. Novaes AB Jr and AB. Novaes, "Soft tissue management for primary closure in guided bone regeneration: surgical technique and case report.," *Int J Oral Maxillofac Implants*, vol. 12, no. 1, pp. 84–87, 1997.
27. M. Zaborowska, A. Bodin, H. Bäckdahl, J. Popp, A. Goldstein, and P. Gatenholm, "Microporous bacterial cellulose as a potential scaffold for bone regeneration," *Acta Biomater*, vol. 6, no. 7, pp. 2540–2547, Jul. 2010, doi: 10.1016/j.actbio.2010.01.004.
28. P. M. Favi *et al.*, "Cell proliferation, viability, and in vitro differentiation of equine mesenchymal stem cells seeded on bacterial cellulose hydrogel scaffolds," *Materials Science and Engineering C*, vol. 33, no. 4, pp. 1935–1944, 2013, doi: 10.1016/j.msec.2012.12.100.
29. J. M. Holzwarth and P. X. Ma, "Biomimetic nanofibrous scaffolds for bone tissue engineering," *Biomaterials*, vol. 32, no. 36, pp. 9622–9629, 2011, doi: 10.1016/j.biomaterials.2011.09.009.
30. L. Hong, Y. L. Wang, S. R. Jia, Y. Huang, C. Gao, and Y. Z. Wan, "Hydroxyapatite/bacterial cellulose composites synthesized via a biomimetic route," *Mater Lett*, vol. 60, pp. 1710–1713, 2006, doi: 10.1016/j.matlet.2005.12.004.
31. Y. Wan *et al.*, "Synthesis and characterization of hydroxyapatite–bacterial cellulose nanocomposites," *Compos Sci Technol*, vol. 66, no. 11–12, pp. 1825–1832, Sep. 2006, doi: 10.1016/j.compscitech.2005.11.027.
32. C. J. Grande, F. G. Torres, C. M. Gomez, and M. Carmen Bañó, "Nanocomposites of bacterial cellulose/hydroxyapatite for biomedical applications," *Acta Biomater*, vol. 5, pp. 1605–1615, 2009, doi: 10.1016/j.actbio.2009.01.022.
33. N. Tazi *et al.*, "Hydroxyapatite bioactivated bacterial cellulose promotes osteoblast growth and the formation of bone nodules," *AMB Express*, vol. 2, no. 1, pp. 61–71, 2012, doi: 10.1186/2191-0855-2-61.
34. X. Fan *et al.*, "Preparation and characterization of bacterial cellulose microfiber/goat bone apatite composites for bone repair," *J Appl Polym Sci*, vol. 129, no. 2, pp. 595–603, 2013, doi: 10.1002/app.38702.
35. M. Park, D. Lee, and J. Hyun, "Nanocellulose-alginate hydrogel for cell encapsulation," *Carbohydr Polym*, vol. 116, pp. 223–228, 2015, doi: 10.1016/j.carbpol.2014.07.059.
36. H. Bäckdahl, M. Esguerra, D. Delbro, B. Risberg, and P. Gatenholm, "Engineering microporosity in bacterial cellulose scaffolds," *J Tissue Eng Regen Med*, vol. 2, pp. 320–330, 2008, doi: 10.1002/term.97.
37. T. T. Nge and J. Sugiyama, "Surface functional group dependent apatite formation on bacterial cellulose microfibrils network in a simulated body fluid," *J Biomed Mater Res A*, vol. 33, pp. 97–103, 2006, doi: 10.1002/jbm.a.
38. A. Maidaniuc *et al.*, "Induced wettability and surface-volume correlation of composition for bovine bone derived hydroxyapatite particles," *Appl Surf Sci*, vol. 438, pp. 158–166, 2018, doi: 10.1016/j.apsusc.2017.07.074.
39. Y. Yamada, "Transfer of Gluconacetobacter kakiaceti, Gluconacetobacter medellinensis and Gluconacetobacter maltaceti to the genus Komagataeibacter as Komagataeibacter kakiaceti comb. nov., Komagataeibacter medellinensis comb. nov. and Komagataeibacter maltaceti comb.," *Int J Syst Evol Microbiol*, vol. 64, no. Pt 5, pp. 1670–1672, 2014, doi: 10.1099/ijs.0.054494-0.
40. C. Castro *et al.*, "Gluconacetobacter medellinensis sp. nov., cellulose- and non-cellulose-producing acetic acid bacteria isolated from vinegar," *Int J Syst Evol Microbiol*, vol. 63, no. PART3, pp. 1119–1125, 2013, doi: 10.1099/ijs.0.043414-0.
41. A. Cañas-Gutiérrez, E. Martinez-Correa, D. Suárez-Avendaño, D. Arboleda-Toro, and C. Castro-Herazo, "Influence of bacterial nanocellulose surface modification on calcium phosphates precipitation for bone tissue engineering," *Cellulose*, vol. 27, pp. 10747–10763, 2020, doi: 10.1007/s10570-020-03470-6.

42. M. Osorio *et al.*, "Novel surface modification of three-dimensional bacterial nanocellulose with cell-derived adhesion proteins for soft tissue engineering," *Materials Science and Engineering: C*, vol. 100, no. August 2018, pp. 697–705, 2019, doi: 10.1016/j.msec.2019.03.045.
43. E. G. Hafsteinsdóttir, D. A. White, and D. B. Gore, "Effects of freeze e thaw cycling on metal-phosphate formation and stability in single and multi-metal systems," *Environmental Pollution*, vol. 175, pp. 168–177, 2013, doi: 10.1016/j.envpol.2013.01.007.
44. H. Aguiar, S. Chiussi, M. López-Álvarez, P. González, and J. Serra, "Structural characterization of bioceramics and mineralized tissues based on Raman and XRD techniques," *Ceram Int*, vol. 44, no. 1, pp. 495–504, 2018, doi: http://dx.doi.org/10.1016/j.ceramint.2017.09.203.
45. M. Figueiredo, A. Fernando, G. Martins, J. Freitas, F. Judas, and H. Figueiredo, "Effect of the calcination temperature on the composition and microstructure of hydroxyapatite derived from human and animal bone," *Ceram Int*, vol. 36, no. 8, pp. 2383–2393, 2010, doi: 10.1016/j.ceramint.2010.07.016.
46. V. Karageorgiou and D. Kaplan, "Porosity of 3D biomaterial scaffolds and osteogenesis," *Biomaterials*, vol. 26, no. 27, pp. 5474–5491, 2005, doi: 10.1016/j.biomaterials.2005.02.002.
47. M. Osorio *et al.*, "Development of novel three-dimensional scaffolds based on bacterial nanocellulose for tissue engineering and regenerative medicine: Effect of processing methods, pore size, and surface area," *J Biomed Mater Res A*, vol. 107, no. 2, pp. 348–359, 2019, doi: 10.1002/jbm.a.36532.
48. S. A. Hutchens, R. S. Benson, B. R. Evans, H. M. O'Neill, and C. J. Rawn, "Biomimetic synthesis of calcium-deficient hydroxyapatite in a natural hydrogel," *Biomaterials*, vol. 27, no. 26, pp. 4661–4670, 2006, doi: 10.1016/j.biomaterials.2006.04.032.
49. C. Busuioc, M. Stroescu, A. Stoica-Guzun, G. Voicu, and S. I. Jinga, "Fabrication of 3D calcium phosphates based scaffolds using bacterial cellulose as template," *Ceram Int*, vol. 42, no. 14, pp. 15449–15458, 2016, doi: 10.1016/j.ceramint.2016.06.196.
50. K. a. Zimmermann, J. M. Leblanc, K. T. Sheets, R. W. Fox, and P. Gatenholm, "Biomimetic design of a bacterial cellulose/hydroxyapatite nanocomposite for bone healing applications," *Materials Science and Engineering C*, vol. 31, no. 1, pp. 43–49, 2011, doi: 10.1016/j.msec.2009.10.007.
51. A. F. S. Costa, F. C. G. Almeida, G. M. Vinhas, and L. A. Sarubbo, "Production of bacterial cellulose by Gluconacetobacter hansenii using corn steep liquor as nutrient sources," *Front Microbiol*, vol. 8, pp. 1–12, 2017, doi: 10.3389/fmicb.2017.02027.
52. M. J. Glimcher, "The Nature of the Mineral Phase in Bone: Biological and Clinical Implications," in *Metabolic Bone Disease and Clinically Related Disorders*, Woodhead Publishing Limited, 1998, pp. 23–50. doi: 10.1016/B978-012068700-8/50003-7.
53. N. Yin, S. Y. Chen, Y. Ouyang, L. Tang, J. X. Yang, and H. P. Wang, "Biomimetic mineralization synthesis of hydroxyapatite bacterial cellulose nanocomposites," *Progress in Natural Science: Materials International*, vol. 21, no. 6, pp. 472–477, 2011, doi: 10.1016/S1002-0071(12)60085-9.
54. Y. Z. Wan *et al.*, "Biomimetic synthesis of hydroxyapatite/bacterial cellulose nanocomposites for biomedical applications," *Materials Science and Engineering C*, vol. 27, no. 4, pp. 855–864, 2007, doi: 10.1016/j.msec.2006.10.002.
55. W. Querido, A. L. Rossi, A. P. C. Campos, A. M. Rossi, and M. Farina, "Does crystallinity of extracted bone mineral increase over storage time?," *Materials Research*, vol. 16, no. 5, pp. 970–974, 2013, doi: 10.1590/s1516-14392013005000096.
56. P. Alverez-Lloret, a. B. Rodriguez-Navarro, Ch. S. Romanek, K. F. Gaines, and J. Congdon, "Quantitative Analysis of Bone Mineral Using Ftir," *Macla*, vol. 6, pp. 45–47, 2006.
57. S. Shahabi *et al.*, "Effect of gamma irradiation on structural and biological properties of a PLGA-PEG-hydroxyapatite composite," *Scientific World Journal*, vol. 2014, 2014, doi: 10.1155/2014/420616.
58. M. Iijima *et al.*, "Fluoride analysis of apatite crystals with a central planar OCP inclusion: Concerning the role of F- ions on apatite/OCP/apatite structure formation," *Calcif Tissue Int*, vol. 59, no. 5, pp. 377–384, 1996, doi: 10.1007/s002239900143.
59. M. N. Lee *et al.*, "Elevated extracellular calcium ions promote proliferation and migration of mesenchymal stem cells via increasing osteopontin expression," *Exp Mol Med*, vol. 50, no. 11, 2018, doi: 10.1038/s12276-018-0170-6.
60. Z. Shi *et al.*, "In situ nano-assembly of bacterial cellulose–polyaniline composites," *RSC Adv*, vol. 2, no. 1, pp. 1040–1046, 2012, doi: 10.1039/c1ra00719j.
61. N. B. Nardi and L. da Silva Meirelles, "Mesenchymal Stem Cells: Isolation, In Vitro Expansion and Characterization," pp. 249–282, 2008, doi: 10.1007/978-3-540-77855-4_11.
62. H. Storrie and S. I. Stupp, "Cellular response to zinc-containing organoapatite: An in vitro study of proliferation, alkaline phosphatase activity and biomineralization," *Biomaterials*, vol. 26, no. 27, pp. 5492–5499, 2005, doi: 10.1016/j.biomaterials.2005.01.043.
63. J. A. Rey Cubillos, L. Lareo, S. Gutiérrez, and M. Godoy Corredor, "Fosfatasa Alcalina (ALP) y Runx2 en cultivos celulares de osteoblastos estimulados con campo eléctrico," *Revista Med*, vol. 20, no. 2, p. 14, 2012, doi: 10.18359/rmed.1189.

64. M. D. McKee, C. E. Pedraza, and M. T. Kaartinen, "Osteopontin and wound healing in bone," *Cells Tissues Organs*, vol. 194, no. 2–4, pp. 313–319, 2011, doi: 10.1159/000324244.
65. A. Singh, G. Gill, H. Kaur, M. Amhmed, and H. Jakhu, "Role of osteopontin in bone remodeling and orthodontic tooth movement: a review," *Prog Orthod*, vol. 19, no. 1, 2018, doi: 10.1186/s40510-018-0216-2.
66. K. J. Oldknow, V. E. MacRae, and C. Farquharson, "Endocrine role of bone: Recent and emerging perspectives beyond osteocalcin," *Journal of Endocrinology*, vol. 225, no. 1, pp. R1–R19, 2015, doi: 10.1530/JOE-14-0584.
67. A. M. Ferreira, P. Gentile, V. Chiono, and G. Ciardelli, "Collagen for bone tissue regeneration," *Acta Biomater*, vol. 8, no. 9, pp. 3191–3200, 2012, doi: 10.1016/j.actbio.2012.06.014.
68. J. Sun *et al.*, "Conditioned medium from bone marrow mesenchymal stem cells transiently retards osteoblast differentiation by downregulating Runx2," *Cells Tissues Organs*, vol. 196, no. 6, pp. 510–522, 2012, doi: 10.1159/000339245.